Nonlinear Dyn (2016) 84:1399–1416
DOI 10.1007/s11071-015-2578-z

ORIGINAL PAPER

Distributed time-constrained guidance using nonlinear model predictive control

Jiang Zhao · Siyue Zhou · Rui Zhou

Received: 5 June 2015 / Accepted: 18 December 2015 / Published online: 30 December 2015

Abstract The paper presents a new time-constrained guidance approach for the multi-missile network by using the nonlinear model predictive control (MPC) technique. The objective is to coordinate the impact time of a group of interceptor missiles against the stationary target. The framework of a distributed MPC scheme is developed. Each missile is assigned its own finite-horizon optimal control problem (FHOCP) and only shares the information with its neighbors. The solutions of the local FHOCP are obtained by using the improved pigeon-inspired optimization method that serves as a convenient tool to deal with the equality and inequality constraints. Further, a safe distance-based penalty term is integrated into the local cost function to achieve no-fly zone avoidance for the multi-missile network. The numerical simulations show that the distributed MPC scheme is effective to implement the cooperative time-constrained guidance with satisfied accuracy of target capture. The Monte Carlo test also demonstrates the robustness of the proposed guidance approach in consideration of the no-fly zone constraint.

Keywords Missile guidance · Multiple missiles · Cooperative guidance · Distributed algorithms · Model predictive control · Pigeon-inspired optimization · No-fly zone · Impact time

J. Zhao (✉) · S. Zhou · R. Zhou
School of Automation Science and Electrical Engineering, Beihang University, Beijing 100191, China
e-mail: jzhao@buaa.edu.cn

1 Introduction

Numerous autonomous guidance approaches have been developed in the last decade to improve the performance of interceptor missiles for some specific objectives, such as impact time control, impact angle control, minimum time control, and minimum energy control [1–4]. For a single interceptor missile, the above objectives have been achieved with satisfactory accuracy of target capture. And recently, many studies start to focus on the development of cooperative guidance approaches for the multiple-missile network, which have shown better performance than a single interceptor missile, in detecting the maneuvering targets, penetrating the defense systems, and surviving the threats [5–7]. However, it is more difficult to achieve the time-constrained guidance against a given target in light of the different initial conditions as well as the communication limit in the multiple-missile network [8,9].

In the current literature, two typical classes of approaches have been proposed to develop the time-constrained guidance laws for the multi-missile salvo attack. The first class investigates the design of the impact time constraint in the control command for each interceptor missile. In [10], the closed form of the impact time control guidance law (ITCG) is derived on the basis of linear formulation, which can guide a group of missiles to simultaneously intercept a stationary target at a desirable time. In [11], a time-varying navigation gain is discussed to coordinate the impact time of the multi-missile network. Later, an extension

of the ITCG guidance is presented to control both the impact time and angle in [12]. Regarding the above algorithms, it is required that the global information of the time-to-go is available to each group member in the multiple-missile network. To improve the performance of the time-constrained guidance law, the distributed control architecture is developed on the basis of consensus protocols [13]. The consensus theory is also applied to design the cooperative guidance laws by using the discrete topology model [14]. In addition, a biased proportional navigation guidance method (BPNG) is proposed, in which the time-to-go estimation is derived by solving differential equations analytically [15].

The second class employs the leader-follower model to describe the cooperative interception of multiple-missile network. Based on traditional proportional navigation (PN) algorithm, a nonlinear state tracking controller is used to design the leader-follower strategy in order to achieve the time-constrained guidance [16]. Then, the consensus protocols are applied to the design of leader-follower strategy which guarantees that the impact time of each follower can converge to the leader in finite time [17]. In [18], a heterogeneous leader-follower guidance approach is also discussed for multiple-missile network based on the traditional PN algorithm. Further, the virtual leader scheme is also employed to achieve cooperative guidance by transforming the time-constrained guidance problem to the nonlinear tracking problem [19].

In this paper, the nonlinear model predictive control (MPC) technique [20,21] is used to design the cooperative time-constrained guidance for the multi-missile network. The contribution of the manuscript is described in the following: (1) The distributed MPC scheme is developed to coordinate the impact time of the interceptor missiles, each of which only shares information with the neighbors and solves its own local optimization problem; (2) the pigeon-inspired optimization (PIO) method is enhanced with nonlinear equality and inequality constraints and used to formulate the distributed MPC; (3) the safe distance-based penalty term is integrated into the local cost function to achieve no-fly zone avoidance for the multi-missile network. The paper is organized as follows. Section 2 presents the preliminaries to the guidance geometry and nonlinear MPC. In Sect. 3, the design of the cooperative time-constrained guidance approach is proposed in detail. The effectiveness of the proposed distributed algorithm is demonstrated by the numerical simulations in Sect. 4. Finally, concluding remarks are presented in Sect. 6.

2 Preliminary

2.1 Basic assumptions

To simplify the equations of motion for the missile-target engagement, the nonlinear dynamics of the two-dimensional pursuit situation is considered in this paper. We assume that the following conditions are used to facilitate the analysis of the distributed time-constrained guidance approach:

1. Both the interceptor missiles and the target are considered as the geometric points in the planar plane;
2. The seeker and autopilot dynamics of each interceptor missile are much faster in comparison with the guidance loop;
3. The angle of attack of each interceptor missile is small enough to be neglected;
4. The velocity of each interceptor missile is constant and the acceleration input only changes its direction.

2.2 Guidance geometry

Suppose that N_{m} missiles participate in the multi-missile network to simultaneously intercept a stationary target. Under the aforementioned assumptions, the two-dimensional guidance geometry on many-to-one engagement is depicted in Fig. 1.

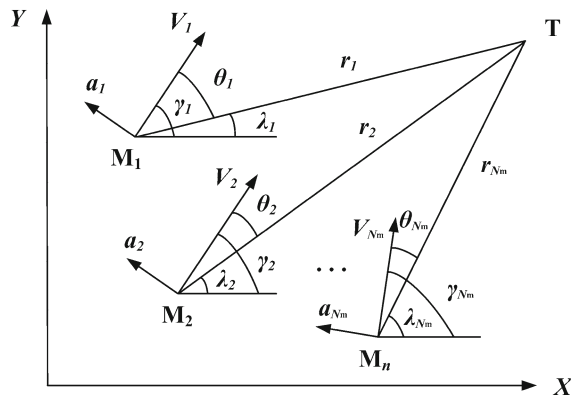

Fig. 1 Guidance geometry on many-to-one engagement

Let M_i denote each interceptor missile and T denote the target. The terms γ_i, λ_i, and θ_i denote the missile heading angle, line-of-sight angle, and look-ahead angle, respectively. As shown in Fig. 1, the look-ahead angle represents the angle between the missile heading angle and line-of-sight angle, which is defined as

$$\theta_i = \gamma_i - \lambda_i \tag{1}$$

where the subscript $i \in \{1, 2, \ldots, N_\mathrm{m}\}$ denotes each member in the multi-missile network. Then, the two-dimensional pursuit situation can be described by the equations of motion in the form of [22]

$$\dot{r}_i = -V_i \cos\theta_i \tag{2}$$

$$\dot{\lambda}_i = -\frac{V_i \sin\theta_i}{r_i} \tag{3}$$

$$\dot{\gamma}_i = \frac{a_i}{V_i} \tag{4}$$

where r_i is the missile-to-target range. V_i is the total velocity of each interceptor missile. The acceleration command is defined as a_i for missile i. The problem studied herein is to find the coordination algorithm that can guide the multi-missile network to the given target at a same time, even if the initial conditions of each member are different.

2.3 Nonlinear MPC

Considering the nonlinear MPC problem, the missile dynamics (1–4) can be written in the equivalent form as follows

$$\dot{z}(t) = f(z(t), u(t)), \quad t \geq t_0, z(0) = z_0 \tag{5}$$

where $z(t) \in \mathcal{R}^n$ is the system state trajectory, and $u(t) \in \mathcal{R}^m$ is the system control trajectory. Then, define the constant prediction horizon as $T_\mathrm{p} \in (0, \infty)$ and the constant control update period as $\delta \in (0, T_\mathrm{p}]$. The common receding horizon update times are given by $t_c = t_0 + \delta c$, $c \in \{0, 1, 2, \ldots\}$. At each time instant t_c, the MPC problem can be formulated by the following finite-horizon optimal control problem (FHOCP).

Problem 1 For each member $i \in \{1, 2, \ldots, N_\mathrm{m}\}$ and at the update time $t_c = t_0 + \delta c$, $c \in \{0, 1, 2, \ldots\}$: Given $z(t_c)$, and then, find

$$u^*(s; t_c) = \arg\min_{u(s;t_c)} J(z(s; t_c), u(s; t_c)) \tag{6}$$

$$J(z(s; t_c), u(s; t_c)) = \int_{t_c}^{t_c+T_\mathrm{p}} F(z(s; t_c), u(s; t_c))\,\mathrm{d}s + \Phi\left(z\left(t_c + T_\mathrm{p}; t_c\right)\right) \tag{7}$$

subject to

$$\dot{z}(s; t_c) = f(z(s; t_c), u(s; t_c)) \tag{8}$$

$$z(s; t_c) \in \mathcal{Z} \tag{9}$$

$$u(s; t_c) \in \mathcal{U} \tag{10}$$

where $s \in [t_c, t_c + T_\mathrm{p}]$ is the prediction horizon. $z(s; t_c)$ and $u(s; t_c)$ are the predicted state trajectory and control trajectory, respectively. $\mathcal{Z}$ and $\mathcal{U}$ are the state and control input constraints. The optimal control trajectory is denoted as $u^*(s; t_c)$. J is the integrated cost function including a running function F and a terminal state penalty function Φ.

3 Time-constrained guidance approach

In this section, the distributed MPC framework in [21] is used to design the time-constrained guidance approach for the multi-missile network. The PIO algorithm is improved to solve the distributed finite-horizon optimal control problem. The main objective is to achieve an agreement on the impact time between each interceptor missile, meanwhile satisfying the no-fly zone constraint.

3.1 Distributed MPC scheme

The decoupled time-invariant nonlinear dynamics for missile i can be written in the equivalent form as

$$\dot{z}_i(t) = f_i(z_i(t), u_i(t)), t \geq t_0 \tag{11}$$

and then, the concatenated vectors in the system (5) can be denoted as $z = (z_1, z_2, \ldots, z_{N\mathrm{m}})$, $u = (u_1, u_2, \ldots, u_{N\mathrm{m}})$, and $f(z, u) = (f_1(z_1, u_1), f_2(z_2, u_2), \ldots, f_{N\mathrm{m}}(z_{N\mathrm{m}}, u_{N\mathrm{m}}))$, respectively.

For the conventional MPC framework in Problem 1, the states of each missile are typically coupled in the integrated cost function to achieve the impact time control. The common components in (7) can be defined as

$$F(z(t), u(t)) = \alpha \sum_{(i,j)\in\mathcal{E}} \left\| t_{\mathrm{go},i}(t) - t_{\mathrm{go},j}(t) \right\|^2 + (1-\alpha) \sum_{i\in\mathcal{V}} \|u_i(t)\|^2 \tag{12}$$

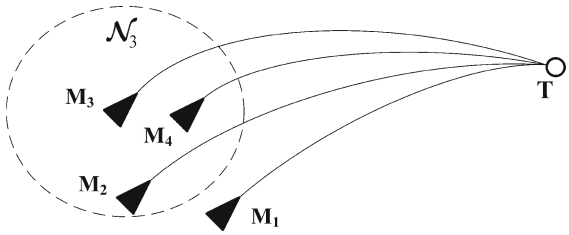

Fig. 2 Example of the communication limitation in the multi-missile network

$$\Phi\left(z\left(t\right)\right)=\beta\sum_{i\in\mathcal{V}}\left\|r_i\left(t\right)\right\|^2 \tag{13}$$

where the symbol $||\cdot||$ denotes any vector norm in $\mathcal{R}^n$. $\mathcal{V}=\{1,2,\ldots,N_{\mathrm{m}}\}$ represents the set of the interceptor missiles. $\mathcal{E}$ is the set of the pair-wise neighbors in the multi-missile network. It is assumed that, if $(i,\,j)\in\mathcal{E}$, then $(j,i)\notin\mathcal{E}$, and $(i,i)\notin\mathcal{E}$ for missile $i\in\mathcal{V}$. The terms α and β are the weighting constants. The time-to-go of each interceptor missile is estimated by the following expression

$$t_{\mathrm{go},i}\left(t\right)=\frac{r_i\left(t\right)}{V_i} \tag{14}$$

The main advantage of the conventional MPC framework is the design of the cost function with (12) and (13) which takes account into the state and control trajectories of all the interceptor missiles. It can reflect overall the motion of the multi-missile network. However, the requirement of computation load is quite high and the guidance approach would be out of work if some interceptor missiles are only able to obtain the effective information from its neighbors. Figure 2 illustrates an example of the communication limitation in the multi-missile network, for which missile i can only communicate with its neighbors in the set $\mathcal{N}_i$. Therefore, the time-constrained guidance should be developed in the distributed framework to achieve an agreement on the impact time.

As shown in Fig. 3, the distributed MPC framework is proposed for the multi-missile network. The main principle is summarized as follows. At each update time, the control inputs of the group of interceptor missiles are first initialized by using the previous predicted optimal control trajectories. Then, each member in the multi-missile network receives the estimated control trajectory from its neighbors, computes the neighbors' states over the current prediction horizon, and meanwhile transmits its estimated control trajectory to the neighbors. Based on the estimated state and control trajectories from neighbors, each missile evaluates the distributed cost function of its own and finds the optimal predicted control trajectory over the current prediction horizon. Finally, the optimal control trajectory over the first control update period is implemented to update the states of each interceptor missile.

To describe the distributed MPC scheme, we first define that the neighbors of each interceptor missile $i\in\mathcal{V}$ have the control vectors $u_{-i}(t)=\{u_j(t)\}$, $j\in\mathcal{N}_i$ and state vectors $z_{-i}(t)=\{z_j(t)\}$, $j\in\mathcal{N}_i$, respectively. The decoupled nonlinear dynamics for the neighbors of missile i can be formulated as

$$\dot{z}_{-i}\left(t\right)=f_{-i}\left(z_{-i}\left(t\right),u_{-i}\left(t\right)\right),\quad t\geq t_0 \tag{15}$$

Then, we define the following notations to distinguish the different kinds of the state and control trajectories for each missile i at current time t_c

(1) $u_i^p\left(s;t_c\right)$, $z_i^p\left(s;t_c\right)$: the predicted control and state trajectories;
(2) $u_i^*\left(s;t_c\right)$, $z_i^*\left(s;t_c\right)$: the optimal predicted control and state trajectories;
(3) $\hat{u}_i\left(s;t_c\right)$, $\hat{z}_i\left(s;t_c\right)$: the estimated control and state trajectories.

where $s\in[t_c,t_c+T_{\mathrm{p}}]$ is the given prediction horizon. Consistent with $u_{-i}(t)$ and $z_{-i}(t)$, the estimated control and state trajectories of the neighbors of each missile i are defined as $\hat{u}_{-i}(s;t_c)$ and $\hat{z}_{-i}(s;t_c)$, respectively.

The estimation of the control trajectory $\hat{u}_{-i}(s;t_c)$ and the state trajectory $\hat{z}_{-i}(s;t_c)$ in the prediction horizon $s\in[t_c,t_c+T_{\mathrm{p}}]$ will be determined at each update time t_c. As shown in Fig. 3, it is typically an iterative process in the proposed distributed MPC scheme by continuously updating the time constant $t_c=t_0+\delta c$, $c\in\{0,1,2,\ldots\}$.

In each iterative process, the estimated control trajectory of its neighboring missile over the prediction horizon $s\in[t_c,t_c+T_{\mathrm{p}}]$ is described according to the aforementioned definition $u_{-i}(t)=\{u_j(t)\}$, $j\in\mathcal{N}_i$. In detail, the estimated control trajectory $\hat{u}_{-i}(s;t_c)$ can be given in the form of

$$\hat{u}_{-i}\left(s;t_c\right)=\left\{\hat{u}_j\left(s;t_c\right)\right\},\ j\in\mathcal{N}_i \tag{16}$$

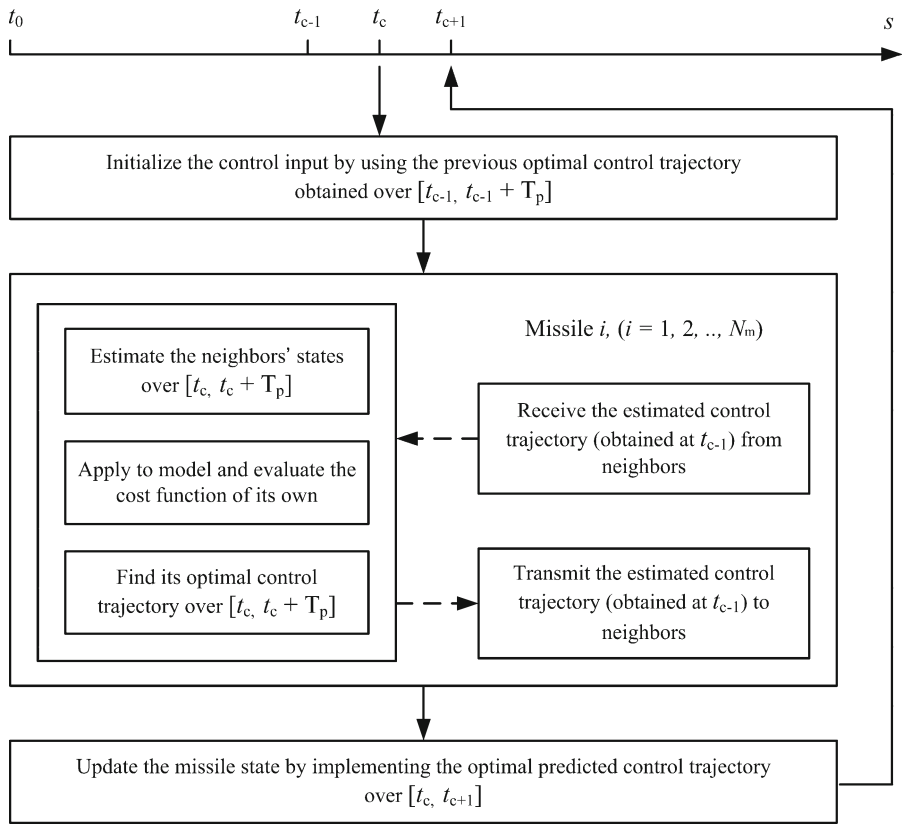

Fig. 3 Framework of the distributed MPC scheme

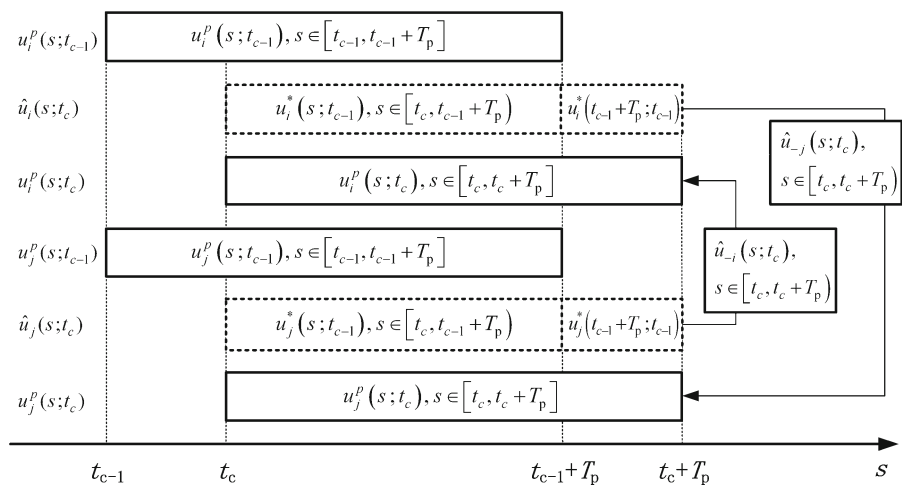

Fig. 4 Generation of the estimated control and state trajectories

where the estimated control trajectory $\hat{u}_j(s;t_c)$ consists of two individual parts over the prediction horizon $s\in[t_c,t_c+T_p]$. As shown in Fig. 4, the first part of the estimated control trajectory $\hat{u}_j(s;t_c)$ inherits the previous optimal control trajectory $u_j^*(s;t_{c-1})$ over the prediction horizon $s\in[t_c,t_{c-1}+T_p)$. The second part of the estimated trajectory $\hat{u}_j(s;t_c)$ over the prediction horizon $s\in[t_{c-1}+T,t_c+T_p]$ is derived from the previous optimal control trajectory $u_j^*(s;t_{c-1})$ at the time instant $s=t_{c-1}+T_p$. To be specific, the estimated control trajectory $\hat{u}_j(s;t_c)$ can be expressed as

$$\hat{u}_j(s;t_c)=\begin{cases} u_j^*(s;t_{c-1}), & s\in[t_c,t_{c-1}+T_p) \\ u_j^*(t_{c-1}+T_p;t_{c-1}), & s\in[t_{c-1}+T_p,t_c+T_p] \end{cases} \tag{17}$$

By using Eqs. (16) and (17), the estimation of the control trajectory of the neighboring missile, $\hat{u}_{-i}(s;t_c)$, is obtained. Then, the relevant state trajectories $\hat{z}_{-i}(s;t_c)$ can be also computed according to the dynamics (15).

Based on the formulation of the estimated control trajectory and state trajectory, the distributed cost function for each missile $i \in \mathcal{V}$ is given in the following expression as

$$\begin{aligned} &F_i\left(z_i^p(s;t_c), \hat{z}_{-i}(s;t_c), u_i^p(s;t_c)\right) \\ &= \alpha \sum_{j\in\mathcal{N}_i} \left\| t_{\mathrm{go},i}^p(s;t_c) - \hat{t}_{\mathrm{go},j}(s;t_c) \right\|^2 \\ &\quad + (1-\alpha)\left\| u_i^p(s;t_c) \right\|^2 \end{aligned} \tag{18}$$

$$\Phi_i\left(z_i^p\left(t_c+T_\mathrm{p};t_c\right)\right) = \beta \left\| r_i\left(t_c+T_\mathrm{p};t_c\right)\right\|^2 \tag{19}$$

where the time-to-go of the neighbors of each missile i is estimated by

$$\hat{t}_{\mathrm{go},j}(s;t_c) = \frac{\hat{r}_j(s;t_c)}{V_j}, \quad j \in \mathcal{N}_i \tag{20}$$

Then, the nonlinear MPC problem at each time instant t_c can be formulated by the distributed FHOCP as follows.

Problem 2 For each member $i \in \{1,2,\ldots,N_\mathrm{m}\}$ and at the update time $t_c = t_0+\delta c,\ c \in \{0,1,2,\ldots\}$: Given $z_i(t_c), z_{-i}(t_c), \hat{u}_i(s;t_c), \hat{u}_{-i}(s;t_c), s\in[t_c, t_c+T_\mathrm{p}]$, and then, find

$$u_i^*(s;t_c) = \arg\min_{u_i(s;t_c)} J_i\left(z_i(s;t_c), z_{-i}(s;t_c), u_i(s;t_c)\right) \tag{21}$$

$$\begin{aligned} &J_i\left(z_i^p(s;t_c), \hat{z}_{-i}(s;t_c), u_i^p(s;t_c)\right) \\ &= \int_{t_c}^{t_c+T_\mathrm{p}} F_i\left(z_i^p(s;t_c), \hat{z}_{-i}(s;t_c), u_i^p(s;t_c)\right) \mathrm{d}s \\ &\quad + \Phi_i\left(z_i^p\left(t_c+T_\mathrm{p};t_c\right)\right) \end{aligned} \tag{22}$$

subject to

$$\dot{z}_i^p(s;t_c) = f_i\left(z_i^p(s;t_c), u_i^p(s;t_c)\right) \tag{23}$$

$$\dot{\hat{z}}_{-i}(s;t_c) = f_{-i}\left(\hat{z}_{-i}(s;t_c), \hat{u}_{-i}(s;t_c)\right) \tag{24}$$

$$z_i^p(s;t_c), \hat{z}_{-i}(s;t_c) \in \mathcal{Z} \tag{25}$$

$$u_i^p(s;t_c), \hat{u}_{-i}(s;t_c) \in \mathcal{U} \tag{26}$$

where $s \in [t_c, t_c+T_\mathrm{p}]$ is the prediction horizon. J_i is the distributed cost function for each missile i, which includes a running function F_i and a terminal state penalty function Φ_i. The optimal control trajectory of each missile $i \in \mathcal{V}$ is denoted as $u_i^*(s;t_c)$.The pseudo-code of the distributed MPC scheme is listed in Algorithm 1.

Algorithm 1: Pseudo-code of the distributed MPC scheme for each missile $i \in \{1,2,\ldots,N_\mathrm{m}\}$.

1: **// Initialization:** at time t_0
2: Set the parameters of the algorithm: T_p, δ
3: Initialize the state trajectory: $z_i(t_0), z_{-i}(t_0)$
4: Set $\hat{u}_i(s;t_0)=0, \hat{u}_{-i}(s;t_0)=0, s\in[t_0,t_0+T_\mathrm{p}]$ and solve **Problem** 2 for missile i, yielding the optimal predicted control trajectory $u_i^*(s;t_0), s\in[t_0,t_0+T_\mathrm{p}]$
5: Apply the first control input $u_i^*(s;t_0), s\in[t_0,t_1)$
6: **// Main loop:** at any time $t_c = t_0+\delta c, c=\{1,2,\ldots\}$
7: Measure the current state $z_i(t_c)$
8: Transmit $\hat{u}_i(s;t_{c-1}), s\in[t_c, t_{c-1}+T_\mathrm{p}]$ to its every neighbor j
9: Receive $\hat{u}_j(s;t_{c-1}), s\in[t_c, t_{c-1}+T_\mathrm{p}]$ from its every neighbor j and compute the estimated trajectory $\hat{u}_{-i}(s;t_c), \hat{z}_{-i}(s;t_c), s\in[t_c,t_c+T_\mathrm{p}]$
10: Solve **Problem** 2 for missile i, yielding $u_i^*(s;t_c), s\in[t_c,t_c+T_\mathrm{p}]$
11: Apply the first control input $u_i^*(s;t_c), s\in[t_c,t_{c+1})$
12: **// Results**
13: Find the optimal control sequences and generate the complete trajectory
14: Validate the trajectory constraints and terminal conditions

3.2 No-fly zone constraint

As the needs for adaptive guidance and control approaches are increasing, the threat avoidance and geopolitical restriction have been considered for the unmanned aerial vehicles [23], unmanned surface vehicles [24], autonomous underwater vehicles [25], and mobile robots [26]. Regarding the interceptor missiles in a complex environment, the no-fly zone constraint is also indispensable to the development of the guidance and control systems. For this reason, recent studies have focused on the design of reference routes [27] and guidance laws [1] in consideration of the no-fly zone constraint. However, only the single interceptor missile was considered in the above work. To improve the performance of multi-missile network in detecting the targets and penetrating the defense systems, the no-fly zone constraint is discussed in this section which enhances the time-constrained cooperative guidance.

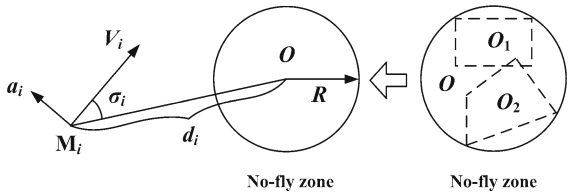

Fig. 5 Geometry on the interceptor missile with no-fly zone constraint

Figure 5 shows the geometry of the interceptor missile with no-fly zone constraint. Herein, the circle-shaped no-fly zone is used because any irregularly shaped no-fly zone can be simply replaced with it. The term R represents the radius of the no-fly zone, and d_i is the distance between the no-fly zone and missile i. The angle $\sigma_i \in (-\pi, +\pi)$ is defined in the line-of-sight frame with respect to the center of the no-fly zone. It can be found that the no-fly zone constraint will possibly be violated as $d_i \to R$ and $|\alpha_i| \to 0$, whereas some larger d_i or $|\alpha_i|$ may protect the interceptor missile against penetrating the no-fly zone.

In the paper, the term d_{safe} is employed to describe the safe distance between each missile and the center of the no-fly zone. The different cases of the interceptor missile in relation to the no-fly zone are illustrated in Fig. 6. To satisfy the no-fly zone constraint, the basic rule, as mentioned above, is to prevent each missile from approaching and pointing to the center of the no-fly zone. Therefore, the terms d_i or $|\alpha_i|$ are used to design the switching conditions under which the members in the multi-missile network must react immediately. As shown in Fig. 6, it is considered that the no-fly zone constraint will be included in the optimization problem when any missile i approaches within the unsafe distance (i.e., $d_i < d_{safe}$) and toward near the center of the no-fly zone (i.e., $|\alpha_i| < \pi/2$). In other words, the interceptor missile will start to adjust its acceleration command for no-fly zone avoidance only when the two conditions above are satisfied.

Thus, the no-fly zone constraint can be solved by adding a penalty term to the distributed cost function. The cost function for each missile i is given by

$$\tilde{J}_i = J_i + \mu \frac{D\left(d_i, \sigma_i\right) \cos \sigma_i}{\|d_i\|^2} \tag{27}$$

where μ is the weighting constant. The term $D(d_i, \sigma_i)$ is determined when the penalty term should be included in the cost function. The detailed form is described as

$$D\left(d_i, \sigma_i\right) = \begin{cases} 1, d_i < d_{\text{safe}} \text{ and } |\sigma_i| < \pi/2 \\ 0, d_i \geq d_{\text{safe}} \text{ or } |\sigma_i| \geq \pi/2 \end{cases} \tag{28}$$

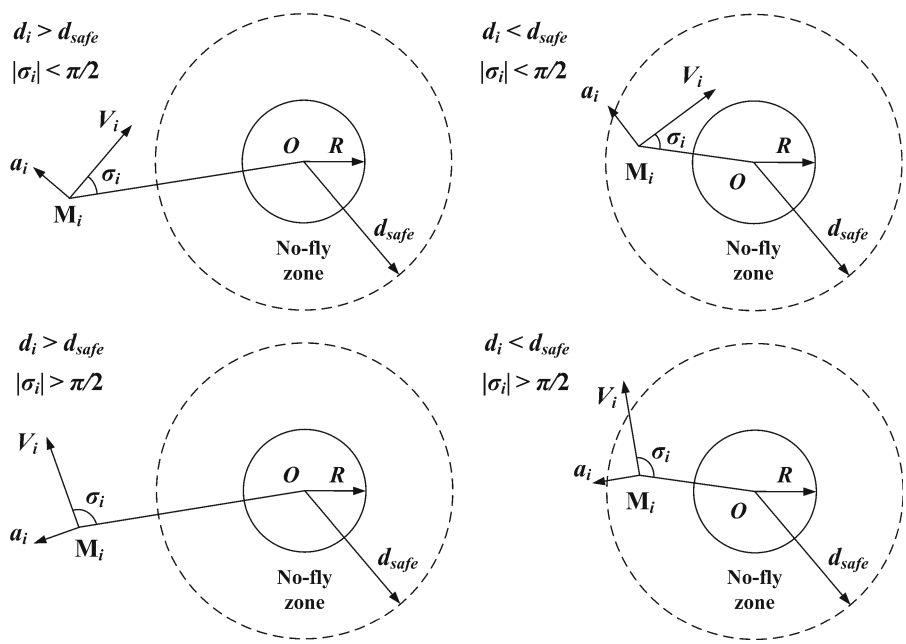

Fig. 6 Different cases of the interceptor missile in relation to the no-fly zone

3.3 Constrained PIO solver

The basic PIO algorithm and its improved version are introduced in this part. The PIO is one of the swarm intelligence (SI)-based methods that take the original inspiration from the natural phenomena. It mimics the motion of a flock of pigeons when they find their home by using the magnetic field, the sun, and the landmarks [28]. As a population-based optimization tool, the PIO has a main strength that each pigeon uses the experience of the whole flock in the search space rather than only the experience of its own. It consists of two individual operators: 1) the map and compass operator; 2) the landmark operator [29]. To be specific, a flock of pigeons first shape the map by using the magnetic field and adjusting the direction according to the altitude of the sun. Then, they will fly close to the destination by using the landmarks neighboring them.

Regarding the basic PIO solver, the total population of pigeons is given by N_p. The dimension of the problem to be solved is defined as N_d. Each pigeon in the flock represents a possible solution and corresponds to a specific value of the fitness function. The number of the iterations is N_iter. The initial set of the pigeons is randomly selected in the searching space. The pigeon p is associated with a position vector $X(p)$ and a velocity vector $Y(p)$ in the form of

$$X(p) = [x_1(p), x_2(p), \ldots, x_{N_\mathrm{d}}(p)], \times (p = 1, 2, \ldots, N_\mathrm{p}) \tag{29}$$

$$Y(p) = [y_1(p), y_2(p), \ldots, y_{N_\mathrm{d}}(p)], \times (p = 1, 2, \ldots, N_\mathrm{p}) \tag{30}$$

In the map and compass operator, all the pigeons try to adjust and follow the best position in the flock. The position vector $X(p)$ and the velocity vector $Y(p)$ are updated by the following equations [28]:

$$Y^{(\mathrm{iter}+1)}(p) = Y^{(\mathrm{iter})}(p) \cdot e^{-\omega_\mathrm{p}(\mathrm{iter}+1)} + \mathrm{rand} \cdot \left(B^{(\mathrm{iter})} - X^{(\mathrm{iter})}(p)\right) \tag{31}$$

$$X^{(\mathrm{iter}+1)}(p) = X^{(\mathrm{iter})}(p) + Y^{(\mathrm{iter}+1)}(p) \tag{32}$$

where iter(iter $= 1, 2, \ldots, N_\mathrm{iter}$) represents each iteration. ω_p is the map and compass factor that influences the velocity of each pigeon. $B^{(\mathrm{iter}-1)}$ denotes the best position in the pigeon flock. *rand* is a random number within [0, 1].

In the landmark operator, half flock of the pigeons (they are away from the landmarks) is driven to follow the other half (they are close to the landmarks). The selected half of pigeons will guide the whole flock to the destination. The center of these pigeons can be obtained by [28]

$$C^{(\mathrm{iter}+1)} = \frac{\sum_{N_\mathrm{P}} X^{(\mathrm{iter}+1)}(p) \cdot \mathrm{fitness}\left(X^{(\mathrm{iter}+1)}(p)\right)}{\sum \mathrm{fitness}\left(X^{(\mathrm{iter}+1)}(p)\right)} \tag{33}$$

where *fitness* $(\cdot)$ reflects the cost function of the problem. The number of pigeons in the current iteration is updated in the form of

$$N_\mathrm{p}^{(\mathrm{iter}+1)} = \frac{1}{2} N_\mathrm{p}^{(\mathrm{iter})} \tag{34}$$

Thus, in this landmark operator, the position vector is manipulated by the following equation:

$$X^{(\mathrm{iter}+1)}(p) = X^{(\mathrm{iter})}(p) + \mathrm{rand} \cdot \left(C^{(\mathrm{iter}+1)} - X^{(\mathrm{iter})}(p)\right) \tag{35}$$

To improve the performance of the basic PIO algorithm (29–35), the paper expands its further application to the parameter optimization problem that includes many nonlinear path constraints and terminal conditions. First, the components of each possible solution in the PIO will be constrained in their respective ranges. To be specific, the position component is bounded in the form of

$$\mathrm{la}_k \le x_k^{(\mathrm{iter})}(p) \le \mathrm{lb}_k, (k = 1, 2, \ldots, N_\mathrm{d}) \tag{36}$$

where la_k and lb_k are the given constants. The corresponding velocity vector should also be limited to suitable range; otherwise the update of the map and compass operator would violate the constraint (36). It has the expression as

$$-\mathrm{ld}_k \le y_k^{(\mathrm{iter})}(p) \le \mathrm{ld}_k, \mathrm{ld}_k = \mathrm{lb}_k - \mathrm{la}_k, (k = 1, 2, \ldots, N_\mathrm{d}) \tag{37}$$

Thus, the following rules are derived for the update laws (31, 32), which can guarantee that the position vector $X(p)$ and the velocity vector $Y(p)$ are constrained by (36, 37)

(a) If $y_k^{(\mathrm{iter})}(p) < -\mathrm{ld}_k \Rightarrow y_k^{(\mathrm{iter})}(p) = -\mathrm{ld}_k$.
(b) If $y_k^{(\mathrm{iter})}(p) > \mathrm{ld}_k \Rightarrow y_k^{(\mathrm{iter})}(p) = \mathrm{ld}_k$.

(c) If $x_k^{(\text{iter})}(p) < \text{la}_k \Rightarrow x_k^{(\text{iter})}(p) = \text{la}_k$ and $y_k^{(\text{iter})}(p) = 0$.

(d) If $x_k^{(\text{iter})}(p) > \text{lb}_k \Rightarrow x_k^{(\text{iter})}(p) = \text{lb}_k$ and $y_k^{(\text{iter})}(p) = 0$.

Next, the equality and inequality constraints will also be involved in the PIO solver to meet the requirement of the constrained optimization problem. Considering the position vector $X(p)$, the typical expressions of equality and inequality constraints are described in the form of

$$\varphi_m(X(p)) = 0, (m = 1, 2, \ldots, N_1) \tag{38}$$

$$\xi_q(X(p)) \leq 0, (q = 1, 2, \ldots, N_2) \tag{39}$$

where N_1 and N_2 are the numbers of the equality and inequality constraints, respectively.

For the equality constraints, many SI-based algorithms use the popular solution by adding the penalty terms to the fitness function, which is also employed in the PIO solver. Thus, the fitness function consists of the basic cost function J and the equality constraints (38) as follows

$$\text{Fitness}(X(p)) = \min_{X(p)} \tilde{J} = J + \sum_{m=1}^{N_1} \omega_m \|\varphi_m(X(p))\|^2 \tag{40}$$

where $\omega_\text{m} \geq 0$ are the weighting constants. Note that the selection of ω_m usually depends on the actual optimization problem.

For the inequality constraints, the problem is less intractable even though they narrow the searching space of the feasible solutions. Because the inequality constraints do not decrease the degree of freedom (DOF) of the optimization problem, a simple approach is used herein by setting the fitness function to an infinite value if some members in the pigeon flock violate any inequality constraint. In detail, the following rule is derived to satisfy the constraint (39)

(e) If $\xi_q(X(p)) > 0 \Rightarrow \text{fitness}(X(p)) = \infty$ and $Y(p) = 0$.

In the above rule, the related velocity vector is also set to zero such that the flock of pigeons would not be affected by the velocity update if some inequality constraints are violated. The other steps of iterations are similar to the basic PIO. The complete pseudo-code of the proposed PIO solver is listed in Algorithm 2.

Algorithm 2: Pseudo-code of the constrained PIO solver

```
// Initialization
Set the parameters of the algorithm:
  N_d, N_p, N_iter, ω_p, la_k, lb_k
Generate N_p random pigeons with position vector
  X(p) and velocity vector Y(p)
Formulate the fitness function on the basis of (22)
// Main loop
while iteration iter ≤ N_iter (stop criteria)do
// The map and compass operator
for N_p pigeonsdo
Update pigeon velocity using (31)
Update pigeon position using (32)
Evaluate the fitness and determine the current best
  position
end for
// The landmark operator
Rank the fitness and select the half flock of pigeons
  close to the landmarks
Determine the center of the selected half using (33)
  and (34)
Update pigeon position using (35)
end while
// Results
Find the global best position, i.e., the optimal solution
```

4 Numerical simulations

4.1 Example 1 (cooperative engagement)

In this part, a simulation scenario of cooperative engagement is performed to demonstrate the effectiveness of the proposed time-constrained guidance approach. Suppose that a group of three missiles intercept a stationary target at (0, 0). The position of each missile $i \in \{1, 2, 3\}$ in the inertial reference frame can be obtained by

$$\dot{x}_i = V_i \cos\gamma_i, \dot{y}_i = V_i \sin\gamma_i \tag{41}$$

where x_i and y_i are the downrange and the crossrange, respectively. As shown in Fig. 7, a simple communication topology is selected for the multi-missile network. To be specific, missile 1 and missile 3 can only obtain the information from the neighbor missile 2, i.e., $\mathcal{N}_1 = \{2\}$, $\mathcal{N}_2 = \{1, 3\}$, and $\mathcal{N}_3 = \{2\}$. Table 1 presents the initial conditions of interceptor missiles. The acceleration of each member in the multi-missile network is limited within $\pm 5.0 \times 9.81$ m/s^2.

In case 1, the acceleration rate of each missile is not limited. The constant prediction horizon is set to

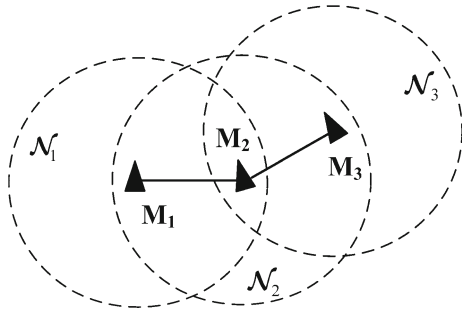

Fig. 7 Communication topology for the multi-missile network

Table 1 Initial conditions of the interceptor missiles

Missiles	x (m)	y (m)	γ (°)	V (m/s)
Missile 1	−1200	−3800	120	235
Missile 2	−4200	−1500	60	240
Missile 3	−4000	2500	15	245

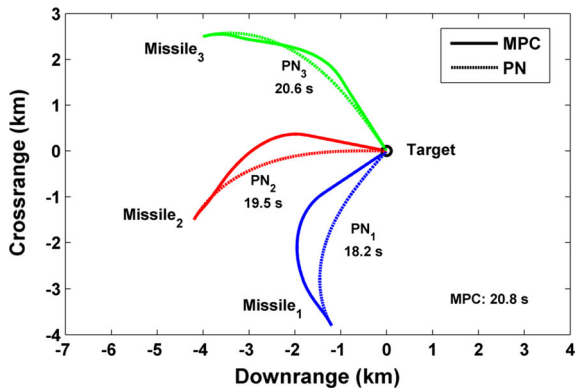

Fig. 8 Ground tracks of the interceptor missiles in case 1

$T_\mathrm{p} = 0.4$ s and the constant control update period is set to $\delta = 0.1$ s. Figures 8 and 9 present the simulation results of the proposed time-constrained guidance approach in comparison with the traditional PN algorithm. The navigation constant for each missile is set to 3.0. As shown in Fig. 8, the final impact time of the three missiles by using the PN algorithm is 18.2, 19.5, and 20.6 s, respectively. The ground tracks obtained by using the distributed MPC scheme illustrate that both missile 2 and missile 3 move farther rounds to achieve a simultaneous interception on the target. The final impact time of the multi-missile network reaches an agreement on 20.8 s, which shows the feasibility of the time-constrained guidance.

Then, we define the nominal time-to-go error of each member in the multi-missile network as follows

$$e_{t,i} = \sum_{j \in \mathcal{N}_i} \left\| t^p_{\mathrm{go},i} - \hat{t}_{\mathrm{go},j} \right\|^2 \tag{42}$$

It can be found that the time-to-go error of each interceptor missile i converges to zero before $t = 5$ s, as shown in Fig. 9. The acceleration commands of the interceptor missiles also decrease to around zero as they gradually approach the given target. The effectiveness of the proposed distributed MPC scheme is demonstrated.

In case 2, the limit of the acceleration rate is taken into account for each missile in the multi-missile network. To evaluate the proposed guidance approach, the different constant control update period is selected as $\delta = 0.1$ s and $\delta = 0.05$ s, respectively. The constant prediction horizon is still set to $T_\mathrm{p} = 0.4$ s. Figure 10 presents the ground tracks of the three interceptor missiles. The numerical trajectories obtained by using $\delta = 0.1$ s are quite similar to the trajectories by using $\delta = 0.05$ s. However, the smaller control update period $\delta = 0.05$ s leads to a faster convergence of the time-to-go error than the period $\delta = 0.1$ s, as shown in Figs. 11 and 12. In return, the control effort of each missile with $\delta = 0.05$ s is larger than that with $\delta = 0.1$ s.

4.2 Example 2 (cooperative engagement with no-fly zone)

In this example, a simulation scenario of the cooperative engagement with no-fly zone constraint is performed to show the effectiveness of the time-constrained guidance approach. The initial conditions, control limits, and communication topology of the multi-missile network are the same with those in Example 1. The constant prediction horizon and control update period are set to $T_\mathrm{p} = 0.4$ s and $\delta = 0.1$ s, respectively. The center of the no-fly zone is set at (2250 m, 1800 m), and the radius is $R = 400$ m. Note that missile 3 would penetrate the given no-fly zone if the penalty term in (27) is not added to the cost function.

In case 3, the safe distance for avoidance of the no-fly zone is set to $d_\mathrm{safe} = 600$ m and $d_\mathrm{safe} = 500$ m, respectively. Figure 13 illustrates the numerical results of the ground tracks of interceptor missiles. It can be found that the no-fly zone constraint is satisfied by using the

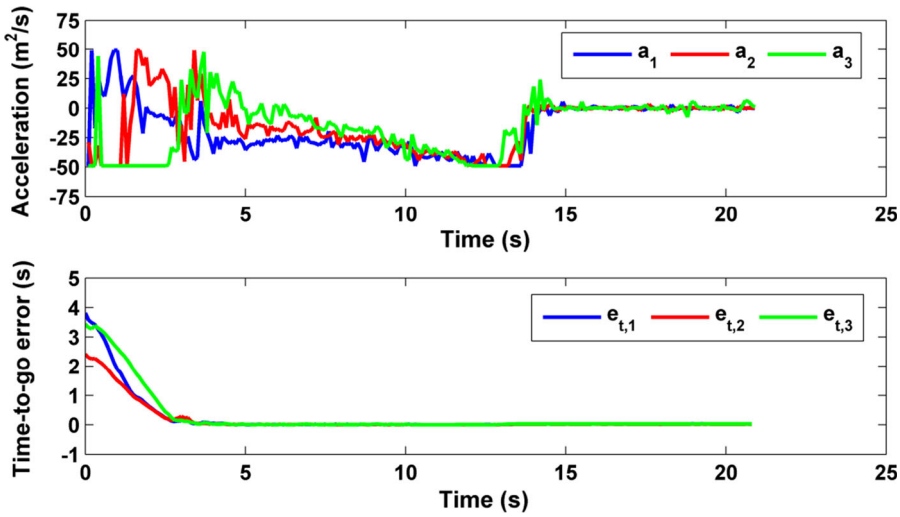

Fig. 9 Histories of the accelerations and time-to-go errors in case 1

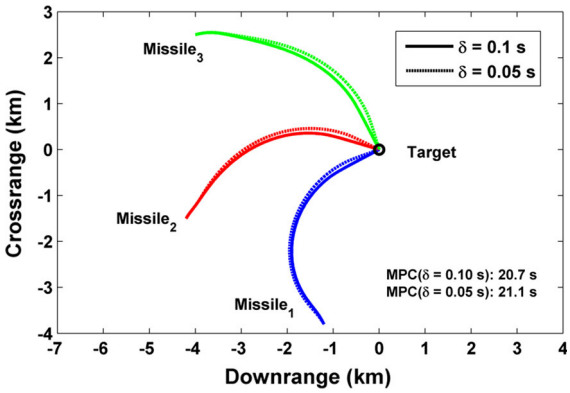

Fig. 10 Ground tracks of the interceptor missiles in case 2

time-constrained guidance algorithm with each safe distance above. However, the ground track of missile 3 is farther away from the no-fly zone when the safe distance $d_{\text{safe}} = 600$ m is selected. In Figs. 14 and 15, the histories of the acceleration commands also show that the larger safe distance d_{safe} results in the earlier saturation of the control effort of missile 3. Although the time-to-go error of the multi-missile network increases slightly as missile 3 moves around the no-fly zone, the convergence of the time-to-go error is not violated. The final impact times of the interceptor missiles reach an agreement on 21.9 s ($d_{\text{safe}} = 600$ m) and 21.1 s (with $d_{\text{safe}} = 500$ m), respectively.

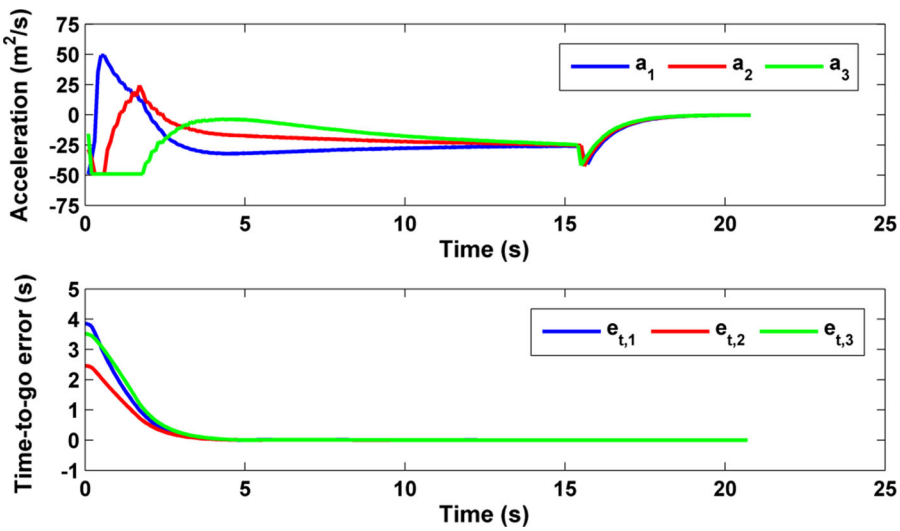

Fig. 11 Histories of the accelerations and time-to-go errors in case 2 ($\delta = 0.1$ s)

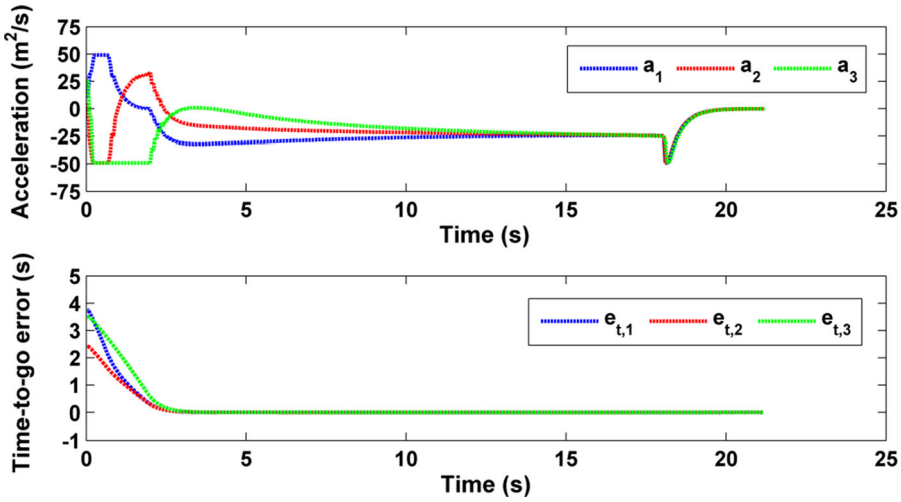

Fig. 12 Histories of the accelerations and time-to-go errors in case 2 ($\delta = 0.05$ s)

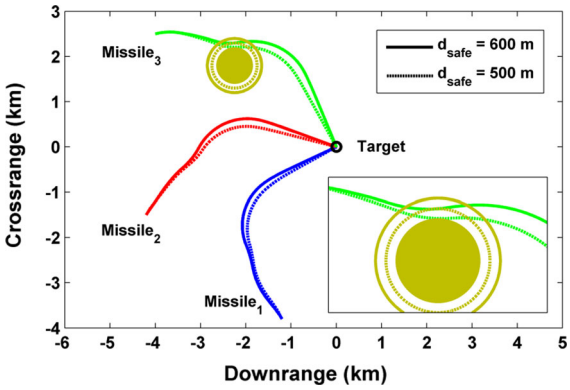

Fig. 13 Ground tracks of the interceptor missiles in case 3

In case 4, the Monte Carlo test is performed to demonstrate the robustness of the proposed distributed MPC scheme. The safe distance is set to $d_{\text{safe}} = 500$ m. Table 2 lists the dispersions that are used in this simulation. Figures 16 and 17 present the numerical results of the Monte Carlo test in 40 times. The ground tracks of interceptor missiles show that the time-constrained guidance is achieved with satisfied accuracy of target capture. The final impact times range from 20.9 to 23.1 s in the simulation. The Monte Carlo results also demonstrate that the no-fly zone constraint can be solved by means of a penalty term into the cost function.

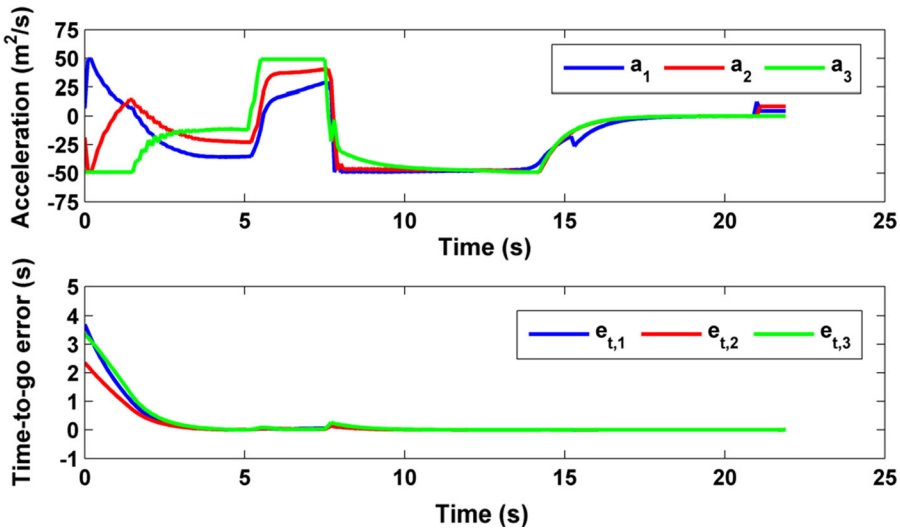

Fig. 14 Histories of the accelerations and time-to-go errors in case 3 ($d_{\text{safe}} = 600$ m)

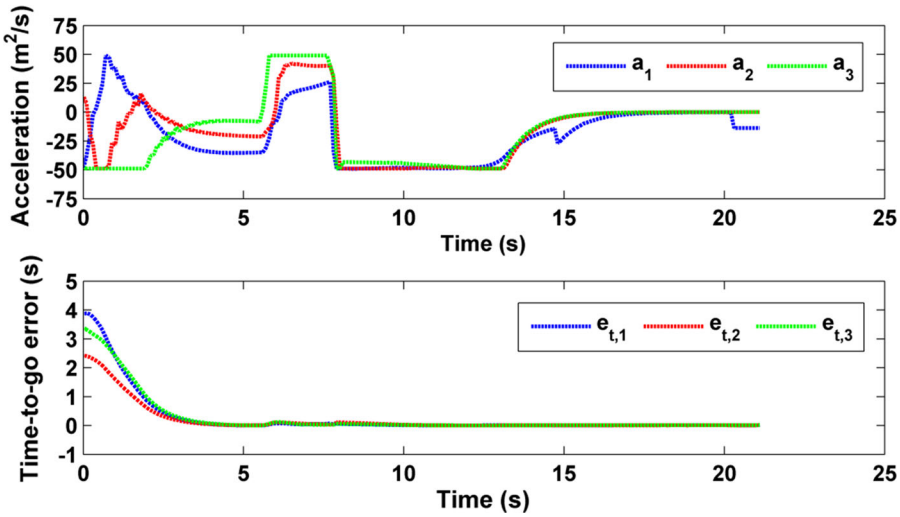

Fig. 15 Histories of the accelerations and time-to-go errors in case 3 ($d_{\text{safe}} = 500$ m)

Table 2 Dispersions used in the Monte Carlo test

Parameters	x (m)	y (m)	γ (°)
Uniform dispersion	±200	±200	±5

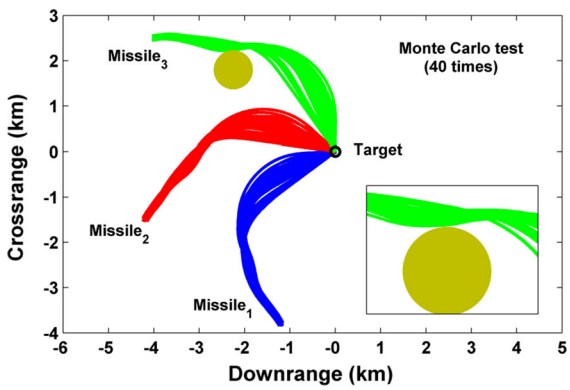

Fig. 16 Ground tracks of the interceptor missiles in case 4

5 Discussions

5.1 Large initial heading errors

In this part, the time-constrained guidance of the interceptor missiles with some large initial heading errors is performed to show the effectiveness of the proposed MPC scheme. The initial conditions of the interceptors and target are same with those in Sect. 4.1. The initial heading of missile 1 is set to $\gamma_1 = 90°$, $\gamma_1 = 120°$, $\gamma_1 = 150°$, and $\gamma_1 = 180°$. Thus, the initial heading errors between missile 1 and missile 3 are $\Delta\gamma_{13} = 75°$, $\Delta\gamma_{13} = 105°$, $\Delta\gamma_{13} = 135°$, and $\Delta\gamma_{13} = 165°$, respectively.

Figures 18 and 19 illustrate the numerical results of ground tracks and accelerations. With different initial heading errors, the interceptor missiles can achieve the simultaneous impact on the given target in the above four cases. It can be found that a larger initial heading error ($\gamma_1 = 180°$, $\Delta\gamma_{13} = 165°$) typically leads to the farther ground tracks of missile 2 and missile 3. As shown in Fig. 19, the acceleration commands also decrease to around zero as the interceptor missiles gradually approach the given target. The histories of the times-to-go with large initial heading errors are presented in Fig. 20. It demonstrates that the convergence of the impact time between each interceptor missile can be guaranteed by the distributed MPC scheme.

5.2 Autopilot dynamics

The autopilot dynamics may influence the performance of the time-constrained guidance scheme. In this part, the PIO-based MPC method is tested in consideration of autopilot lags. The autopilot dynamics can be usually described by the first-order differential equations in the form of

$$\dot{a}_{Mi} = -\frac{1}{\tau}a_{Mi} + \frac{1}{\tau}a_i \tag{43}$$

where τ is the time constant of the autopilot, and a_i is the command to the autopilot.

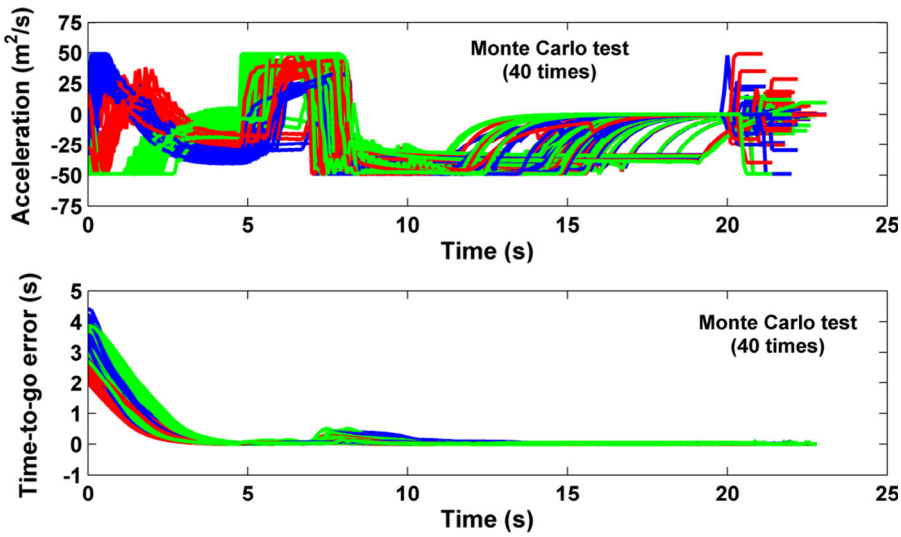

Fig. 17 Histories of the accelerations and time-to-go errors in case 4

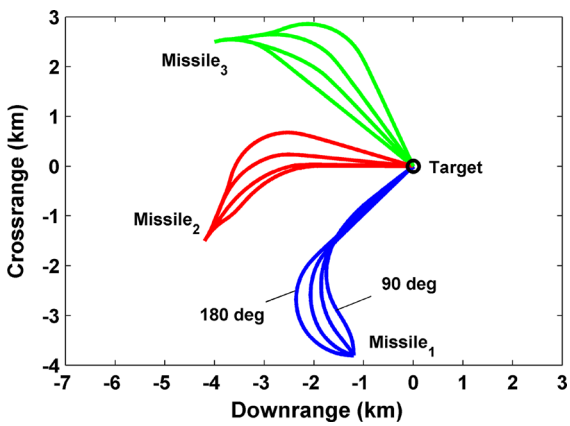

Fig. 18 Ground tracks with large initial heading errors ($\gamma_1 = 90°, 120°, 150°, 180°$; $\Delta\gamma_{13} = 75°, 105°, 135°, 165°$)

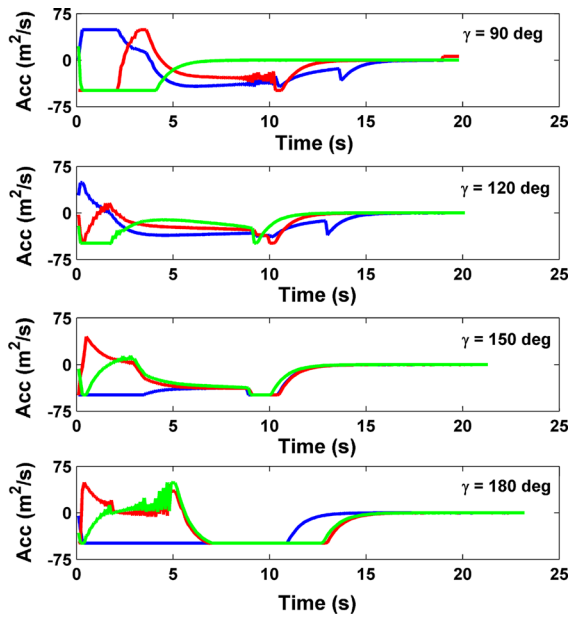

Fig. 19 Accelerations with large initial heading errors ($\gamma_1 = 90°, 120°, 150°, 180°$; $\Delta\gamma_{13} = 75°, 105°, 135°, 165°$)

The dynamics (43) is added in each control update period (not in the prediction model) to test the distributed MPC scheme. The time constant of the autopilot is set to $\tau = 0.5$ and $\tau = 1.0$, respectively. The initial conditions of the interceptor missiles are same with those in Sect. 4.1. The numerical results of the ground tracks are illustrated in Fig. 21. The histories of the accelerations and times-to-go with different autopilot lags are presented in Figs. 22 and 23. It can be found that the interceptor missiles with time constant $\tau = 1.0$ move farther rounds to achieve a simultaneous impact on the target. Each interceptor missile typically requires longer time to respond to the guidance commands with the time constant $\tau = 1.0$ than $\tau = 0.5$. As shown in Fig. 23, it also demonstrates that a larger time constant of the autopilot results in a slower convergence of the times-to-go.

5.3 Environmental disturbances

The environmental disturbances may also have an impact on the performance of guidance system. Therefore, the simulation scenario of cooperative engage-

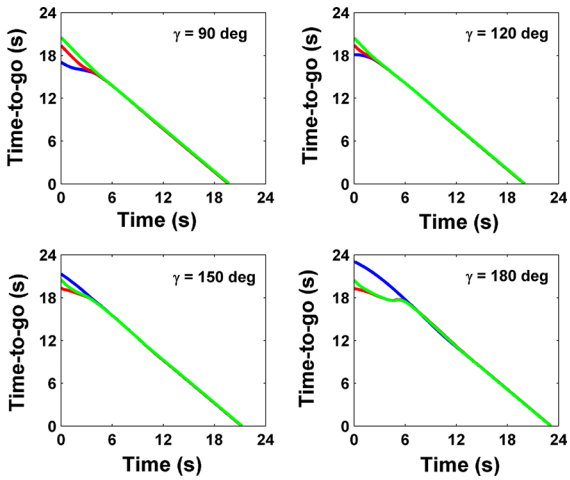

Fig. 20 Times-to-go with large initial heading errors ($\gamma_1 = 90°, 120°, 150°, 180°$; $\Delta\gamma_{13} = 75°, 105°, 135°, 165°$)

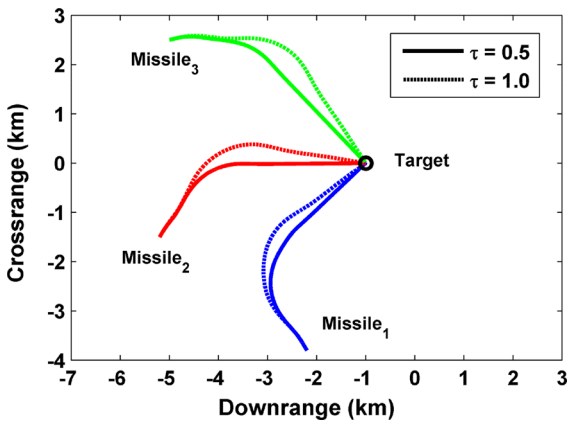

Fig. 21 Ground tracks with different autopilot lags ($\tau = 0.5$, 1.0)

ment in consideration of wind disturbances is performed to show the effectiveness of the distributed MPC scheme. The model of the bounded wind disturbances can be described as

$$\dot{x}_i = V_i \cos\gamma_i + W_x,\ \dot{y}_i = V_i \sin\gamma_i + W_y,\ |W_x| \le W_{\max},\ |W_y| \le W_{\max} \tag{44}$$

where W_x and W_y are the components of the wind velocity, and $W_{\max}$ is the maximum magnitude of W_x and W_y.

Similarly, the bounded wind disturbances (44) are included in each control update period (not in the prediction model) to test the guidance approach. The initial conditions of interceptor missiles are same with those in Sect. 4.1. The bounded wind disturbances are

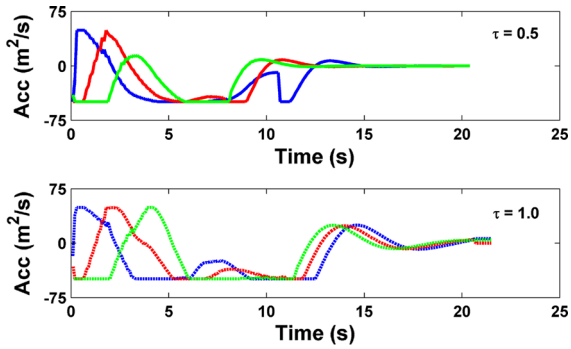

Fig. 22 Accelerations with different autopilot lags ($\tau = 0.5$, 1.0)

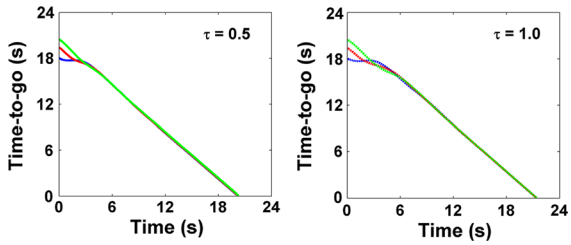

Fig. 23 Times-to-go with different autopilot lags ($\tau = 0.5$, 1.0)

set to $W_{\max} = 10$ m/s, $W_{\max} = 20$ m/s, and $W_{\max} = 30$ m/s, respectively. Figures 24, 25, and 26 present the numerical results of the ground tracks, accelerations, and times-to-go of each interceptor missile. It can be found that the cooperative guidance can be achieved by using the PIO-based MPC scheme in consideration of some weak wind disturbances such as $W_{\max} = 10$ m/s and $W_{\max} = 20$ m/s. Typically, the wind disturbance $W_{\max} = 20$ m/s leads to larger terminal accelerations than the disturbance $W_{\max} = 10$ m/s. As shown in Figs. 24 and 26, the interceptor missiles fail to converge to the given target at a constant final time when the strong wind disturbance ($W_{\max} = 30$ m/s) is included in the guidance system. In this case, the estimation of the disturbances should be considered in the prediction model for disturbance rejection.

5.4 Computation efficiency

The PIO parameters, control update period, and prediction horizon typically determine the success rate of the time-constrained guidance approach. Therefore, this part will discuss the computation efficiency of the proposed MPC scheme.

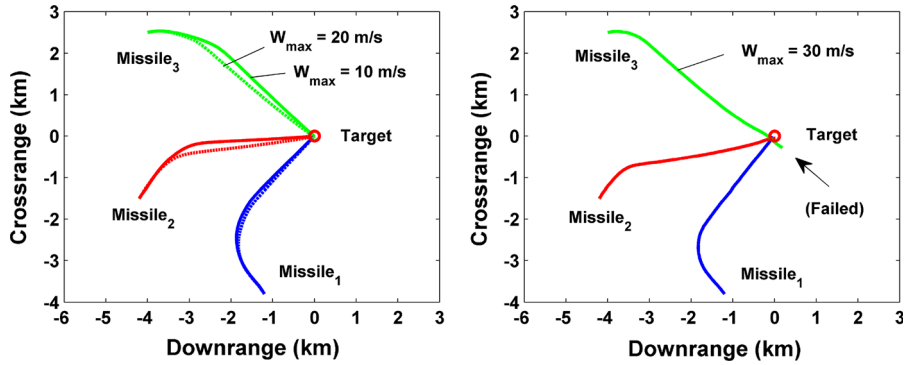

Fig. 24 Ground tracks with different wind disturbances ($W_{\max} = 10$ m/s, 20 m/s, 30 m/s)

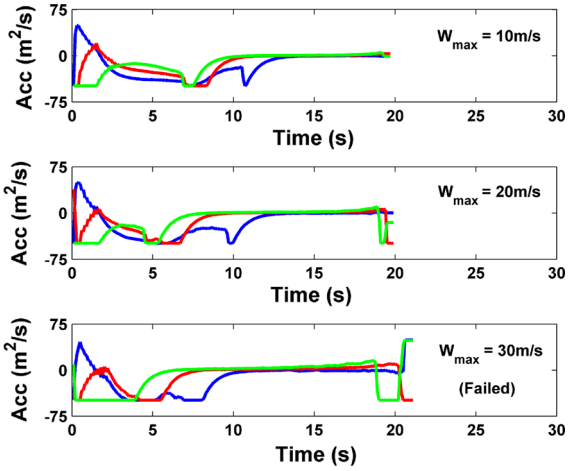

Fig. 25 Accelerations with different wind disturbances ($W_{\max} = 10$ m/s, 20 m/s, 30 m/s)

Using the standard Visual C++, the simulations are run for several cases with different PIO parameters, control update period, and prediction horizon. In detail, the pigeon population of the PIO solver is set to $N_p = 30$ and $N_p = 50$. The iteration number is set to $N_{iter} = 30$ and $N_{iter} = 50$. The control update period is set to $\delta = 0.05$ s, $\delta = 0.1$ sec, and $\delta = 0.15$ s, respectively. The prediction horizon is set to $T_{\rm p} = 4\delta$ and $T_{\rm p} = 6\delta$. For each case, the simulation is repeated 30 times with the same parameters. Table 3 shows the statistical results of the PIO-based MPC scheme for comparison.

Table 3 Success rate of the PIO-based MPC scheme (repeated 30 times)

Parameters	Success rate (%): $T_{\rm p} = 4\delta / T_{\rm p} = 6\delta$		
	$\delta = 0.05$ s	$\delta = 0.1$ s	$\delta = 0.15$ s
$N_{\rm p} = 30,\ N_{\rm iter} = 30$	100/96.7	100/100	100/100
$N_{\rm p} = 50,\ N_{\rm iter} = 50$	90.0 /83.3	100/93.3	100/100

It can be found that a large control update period δ typically raises the success rate of the distributed MPC scheme. The success rate for the cases of $\delta = 0.1$ s and $\delta = 0.15$ s almost reach 100%, because the average running time of the PIO solver in each control update period δ is about 0.018 s ($N_p = 30$, $N_{iter} = 30$) and 0.039 s ($N_p = 50$, $N_{iter} = 50$), respectively. The proper selection of the pigeon population N_p and iteration number N_{iter} may also reach a compromise between the performance index and computation efficiency. In addition, the numerical results of the success rate demonstrate that a reasonable reduction of the prediction horizon $T_{\rm p}$ can improve the stability of the MPC scheme.

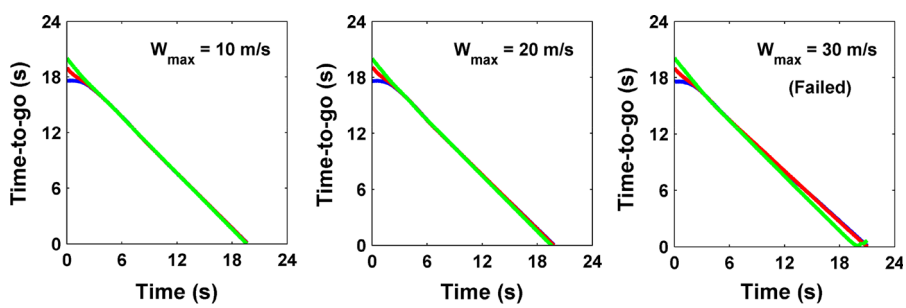

Fig. 26 Times-to-go with different wind disturbances ($W_{\max} = 10$ m/s, 20 m/s, 30 m/s)

6 Conclusions

The cooperative time-constrained guidance with no-fly zone avoidance is studied in this paper. The coordination of impact time for the multi-missile network is achieved by the distributed MPC scheme. The guidance problem is transmitted to the local FHOPC that is solved by the enhanced PIO method. The numerical results show that the acceleration command of each interceptor missile is adjusted by the distributed algorithm to achieve a simultaneous impact on the target. Typically, a smaller control update period δ can lead to a faster convergence of the time-to-go error of the multi-missile network, whereas the control effort will increase in return. The no-fly zone avoidance is also achieved by integrating a safe distance-based penalty term into the local cost function. It shows that a larger safe distance d_{safe} results in the earlier saturation of the control effort. The impacts of large initial heading errors, autopilot lags, and wind disturbances are also discussed to show the effectiveness of the proposed guidance approach. The future work will focus on the design of the time-constrained guidance law against maneuvering targets. The complete three-dimensional guidance geometry should be also taken into consideration to perform the actual cooperative engagement missions.

Acknowledgments The authors would like to thank the editors and the reviewers for their critical and constructive review of this manuscript. This study was co-supported by the National Natural Science Foundation of China (No: 61273349, 61175109) and the Aeronautical Science Foundation of China (No: 2014ZA18004, 2013ZA18001).

References

1. Yu, W., Chen, W.: Guidance law with circular no-fly zone constraint. Nonlinear Dyn. **78**, 1953–1971 (2014)
2. Zhang, Y., Sun, M., Chen, Z.: Finite-time convergent guidance law with impact angle constraint based on sliding-mode control. Nonlinear Dyn. **70**, 619–625 (2012)
3. Zhou, D., Sun, S., Teo, K.L.: Guidance laws with finite time convergence. J. Guid. Control Dyn. **32**(6), 1838–1846 (2009)
4. Zhao, J., Zhou, R.: Unified approach to cooperative guidance laws against stationary and maneuvering targets. Nonlinear Dyn. **81**(4), 1635–1647 (2015)
5. Zhang, Y., Ma, G., Liu, A.: Guidance law with impact time and impact angle constraints. Chin. J. Aeronaut. **26**(4), 960–966 (2013)
6. Zhao, J., Zhou, R., Jin, X.: Progress in reentry trajectory planning for hypersonic vehicle. J. Syst. Eng. Electron. **25**(4), 627–639 (2014)
7. Bao, W.: Present situation and development tendency of aerospace control techniques. Acta Automat. Sin. **39**(6), 697–702 (2013)
8. Zhao, J., Zhou, R., Dong, Z.: Three-dimensional cooperative guidance laws against stationary and maneuvering targets. Chin. J. Aeronaut. **28**(4), 1104–1120 (2015)
9. Zhao, J., Zhou, R.: Reentry trajectory optimization for hypersonic vehicle satisfying complex constraints. Chin. J. Aeronaut. **26**(6), 1544–1553 (2013)
10. Jeon, I.S., Lee, J.I., Tahk, M.J.: Impact-time-control guidance law for anti-ship missiles. IEEE Trans. Control Syst. Technol. **14**(2), 260–266 (2006)
11. Jeon, I.S., Lee, J.I., Tahk, M.J.: Homing guidance law for cooperative attack of multiple missiles. J. Guid. Control Dyn. **33**(1), 275–280 (2010)
12. Lee, J.I., Jeon, I.S., Tahk, M.J.: Guidance law to control impact time and angle. IEEE Trans. Aerosp. Electron. Syst. **43**(1), 301–310 (2007)
13. Zhao, S., Zhou, R.: Cooperative guidance for multimissile salvo attack. Chin. J. Aeronaut. **21**(6), 533–539 (2008)
14. Peng, C., Liu, X., Wu, S., et al.: Consensus problems in distributed cooperative terminal guidance time of multi-missiles. Control Decis. **25**(10), 1557–1566 (2010)
15. Zhang, Y., Ma, G., Wu, H.: A biased proportional navigation guidance law with large impact angle constraint and the time-to-go estimation. Proc. Inst. Mech. Eng. G J. Aerosp. Eng. **228**(10), 1725–1734 (2014)
16. Zhang, Y., Ma, G., Wang, X.: Time cooperative guidance for multi-missiles: a leader–follower strategy. Acta Aeronaut. Astronaut. Sin. **30**(6), 1109–1118 (2009)
17. Sun, X., Zhou, R., et al.: Consensus of leader–followers system of multi-missile with time-delays and switching topologies. Optik **125**(3), 1202–1208 (2014)
18. Zou, L., Ding, Q., Zhou, R.: Distributed cooperative guidance for multiple heterogeneous networked missiles. J. Beijing Univ. Aeronaut. Astronaut. **23**(1), 103–108 (2010)
19. Zhao, S., Zhou, R., Wei, C.: Design of time-constrained guidance laws via virtual leader approach. Chin. J. Aeronaut. **23**(1), 103–108 (2010)
20. Mayne, D.Q.: Model predictive control: recent developments and future promise. Automatica **50**(12), 2967–2986 (2014)
21. Dunbar, W.B., Murray, R.M.: Receding horizon control of multi-vehicle formations: a distributed implementation. IEEE Conference on Decision and Control, Dec 14–17, Atlantis, Paradise Island, Bahamas, pp. 1995–2002 (2004)
22. Zhao, J., Zhou, R.: Obstacle avoidance for multi-missile network via distributed coordination algorithm. Chin. J. Aeronaut. **29**(2) (in press, 2016)
23. Cruz, G.C.S., Encarnacao, P.M.M.: Obstacle avoidance for unmanned aerial vehicles. J. Intell. Robot. Syst. **65**(1–4), 203–217 (2012)
24. Campbell, S., Naeem, W., Irwin, G.W.: A review on improving the autonomy of unmanned surface vehicles through intelligent collision avoidance manoeuvres. Annu. Rev. Control. **36**(2), 267–283 (2012)

25. Fang, M., Wang, S., Mu-Chen, W., et al.: Applying the self-tuning fuzzy control with the image detection technique on the obstacle-avoidance for autonomous underwater vehicles. Ocean Eng. **93**(1), 11–24 (2015)
26. Korayem, M.H., Zehfroosh, A., Tourajizadeh, H., et al.: Optimal motion planning of nonlinear dynamic systems in the presence of obstacles and moving boundaries using SDRE: application on cable-suspended robot. Nonlinear Dyn. **76**(2), 1423–1441(2014)
27. Wang, G., Sun, X., Zhang, L., et al.: Saturation attack based route planning and threat avoidance algorithm for cruise missiles. J. Syst. Eng. Electron. **22**(6), 948–953 (2011)
28. Zhao, J., Zhou, R.: Pigeon-inspired optimization applied to constrained gliding trajectories. Nonlinear Dyn. **82**(4), 1781–1795 (2015)
29. Zhang, B., Duan, H.: Predator–prey pigeon-inspired optimization for UAV three-dimensional path planning. Adv. Swarm Intell. **8795**, 96–105 (2014)